Evaluation of Treatment Response to TNT HEF 2-3-0 Applied to Commercial Soybean Across Early Vegetative Growth Stages on Ebraheim Field

January 2026

Prepared by:

RhizeBio, Inc.™

Prepared for:

TNT Farming Solutions

Executive Summary

This trial evaluated the effects of TNT HEF 2-3-0 in-furrow application on soybean rhizosphere microbiome composition, soil nutrient cycling, and plant nutrient uptake at the Ebraheim Field during the 2025 growing season. Rhizosphere samples were collected at three vegetative growth stages (V2, V4, V7) from treated and control plots (n = 18 total sample sets). Analysis integrated shotgun metagenomic sequencing of root-associated microbial communities, Haney soil chemistry, and plant tissue nutrient analysis to characterize treatment effects across the soil to microbiome to plant nutrient continuum.

The data suggests that areas treated with TNT HEF 2-3-0 exhibited a time-dependent response pattern with pronounced early-season effects that attenuated over time. At V2 and V4, substantial pathogen suppression was observed, with total pathogen occurrence reduced by 42.4% and 46.2%, respectively. Complete elimination was observed for several key soybean pathogens including Diaporthe seed decay (100% reduction), stem canker (100% reduction), and brown spot/Septoria leaf spot (100% reduction). Soybean cyst nematode showed a 75% reduction and charcoal rot declined by 50%.

Soil chemistry analysis revealed significant enhancement of calcium availability in treated soils at V4 (+39.2%, $p = 0.008$), with this effect translating to plant tissue by V7 (+15.6% tissue calcium, $p = 0.014$). Potassium availability showed consistent early-season enhancement (+78.1% at V2, $p = 0.052$; +23.0% at V4, $p = 0.073$). Metagenomic functional profiling identified significant increases in nitrification potential at V4 (+2 percentile points, $p = 0.045$) and phosphorus solubilization potential at V7 (+14 percentile points, $p = 0.013$).

Taxonomic analysis revealed both beneficial and concerning community shifts. Biocontrol fungi increased substantially, with *Trichoderma* showing +129.5% enrichment and overall fungal biocontrol guild increasing +125.1%. Bacterial nutrient cycling guild increased +32.6%. However, the nitrogen-fixing bacterial guild declined by 47.6%, driven primarily by *Bradyrhizobium* reduction (-61.4%), which represents a significant concern for soybean nodulation and biological nitrogen fixation. Mycorrhizal fungi also declined (-25.4%), potentially affecting phosphorus acquisition capacity.

Cross-domain correlation analysis (1,128 pairwise comparisons, 147 significant at $p < 0.05$) identified a consistent pattern of community specialization associated with functional pathway activation. Sulfur oxidation potential showed exceptionally strong inverse correlation with diversity ($r = -0.984$, $p < 0.0001$),

and organic nitrogen breakdown potential correlated positively with tissue nitrogen (r = +0.829, p = 0.006), suggesting a potential mechanistic linkage between microbial function and plant nutrition.

In summary, the data suggests that treatment with TNT HEF 2-3-0 enhanced early-season pathogen suppression, improved calcium nutrition (soil to plant), and stimulated specific microbial functional pathways. Constraints included reduced nitrogen-fixing bacterial populations (-47.6%), late-season pathogen equilibration (+8.8% at V7), and mycorrhizal decline (-25.4%). The nitrogen fixation decline warrants particular attention for soybean production and may benefit from supplemental rhizobium inoculation. Study limitations included small sample size (n = 3 per treatment per stage) and single-site design.

Table of Contents

1. STUDY OVERVIEW

This trial evaluated the effects of in-furrow treatment of soybean crops with TNT HEF 2-3-0 on rhizosphere microbiome composition, soil nutrient cycling, and plant nutrient uptake at Falor Farm Center during the 2025 growing season. TNT Hi Energy Fish was applied in-furrow at planting. Samples were collected from across a single field at three vegetative growth stages: V2 (early vegetative), V4 (mid-vegetative), and V7 (late vegetative). Each growth stage included triplicate samples from treated (TNT HEF 2-3-0) plots and untreted (Control) plots across three field zones (n = 18 total sample sets).

Sampling involved collecting rhizosphere samples including root samples, root-adjacent soil samples, and plant tissue samples. Root samples were analyzed using shotgun metagenomic sequencing to characterize the rhizosphere microbial community and evaluate functional potential. Haney soil chemistry was performed on soils for nutrient availability assessment, and plant tissue was collected for tissue nutrient analysis to quantify nutrient uptake. The integration of these data aims to characterize the complete soil to microbiome to plant nutrient continuum and assess the product's ability to enhance both soil nutrient availability and microbial functionality in facilitating nutrient uptake.

Statistical analyses employed Welch's t-tests for treatment comparisons at each growth stage, with significance thresholds of $p < 0.05$ for statistically significant effects and $p < 0.10$ for marginally significant trends. Correlation analyses across 1,128 pairwise comparisons identified 147 statistically significant cross-domain relationships ($p < 0.05$). The sample size of n = 9 stage-zone paired observations provides adequate statistical power to detect strong correlations ($r > 0.75$), though confidence intervals remain wide.

2. SOIL FERTILITY EFFECTS

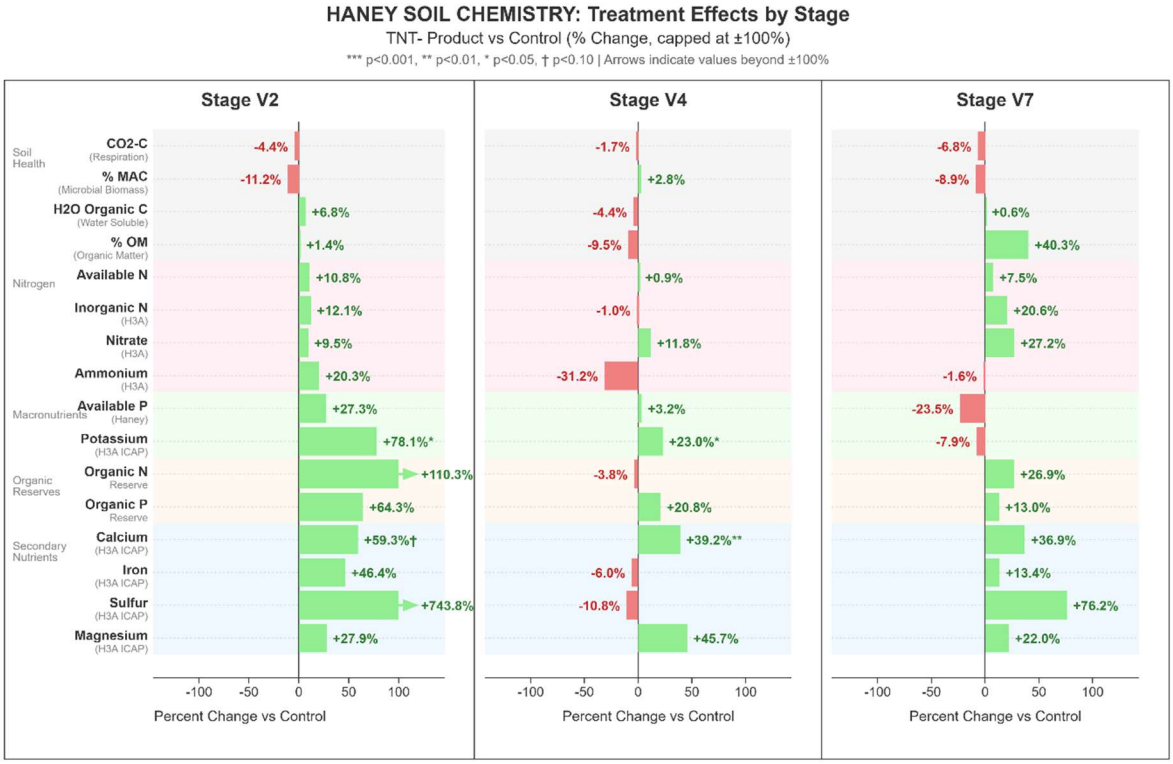

Figure 1. Soil Fertility Chemistry - Treatment Effects by Stage

Soil fertility data revealed dynamic treatment effects on nutrient availability, with enhanced early nutrient levels that stabilized across the growing season but remained marginally elevated by V7, with the most consistent effects observed for calcium and potassium. At V2, soil nutrient pools showed substantial changes in response to treatment, but replicates had high variability that limited statistical power. Treated areas showed increased available nutrients for all primary and secondary nutrients compared to control, notably statistically significant elevate potassium (+78.1%, p = 0.03) and H3A ICAP calcium (+59.3%, p = 0.07). Organic matter remained relatively stable (+1.4%), while soil respiration (CO2-C; -4.4%) and microbial biomass (%MAC; -11.2%) showed modest decreases. These early patterns indicate significant initial treatment effects on mineral nutrient availability with only a minimal disruption to carbon cycling.

By V4, concentrations of most soil nutrients stabilized relative to control. The soil calcium enhancement reached statistical significance, with H3A ICAP calcium increasing by +39.2% (p = 0.004), representing the most robust soil chemistry finding in this trial. Potassium availability persisted at elevated levels (+23.0%, p

= 0.04), though at reduced magnitude compared to V2. Organic matter showed spatial heterogeneity between sampling zones, with Zone 1 increasing (+40%) while Zone 2 decreased (-38.5%). Soil respiration remained near control levels (-1.7%).

At V7, most soil nutrient levels in treated soils rebounded above control levels. Organic matter showed the strongest treatment response (+40.3%), though high variability limited statistical significance (p = 0.18). Soil respiration declined modestly (-6.8%), possibly reflecting the community specialization patterns identified in correlation analysis. Manganese availability was increased substantially in treated soils (+102.2%, p = 0.073, Table 2.1), while zinc showed marginal decline (-24.5%, p = 0.057, Table 2.1). The calcium effects observed at V2 and V4 persisted (+36.9%), while potassium returned to near-control levels (-7.9%).

Table 2.1: Soil Available Nutrient Changes by Growth Stage

Nutrient	V2 Change	V4 Change	V7 Change
H3A ICAP Calcium	+59.3%	+39.2%**	+36.9%
H3A ICAP Potassium	+78.1%	+23.0%	-7.9%
H3A ICAP Manganese	+149.4%	+28.8%	+102.2%
H3A ICAP Zinc	+14.8%	+47.7%	-24.5%
Organic Matter	+1.4%	-9.5%	+40.3%
CO2-C	-4.4%	-1.7%	-6.8%

*Note: ** p < 0.01, * p < 0.05. Values represent percent change (Treatment - Control) / Control.*

3. MICROBIAL FUNCTIONS

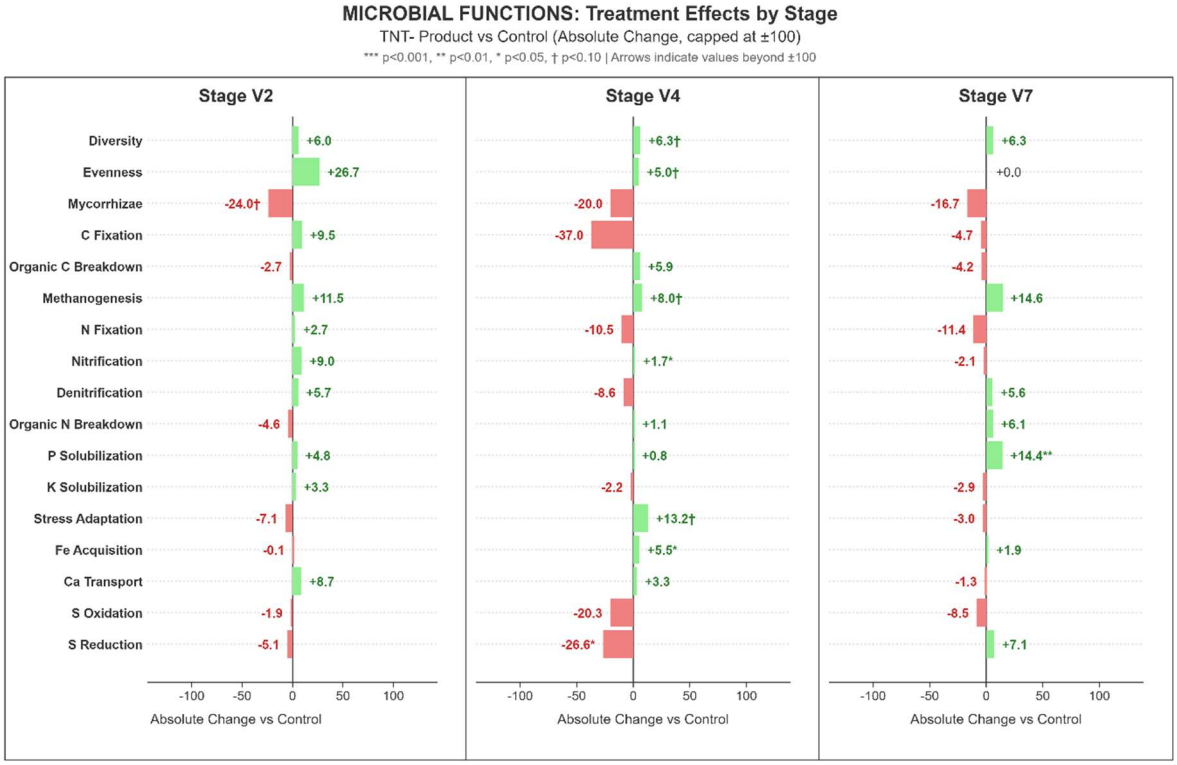

Figure 2. Microbial Functional Pathways - Treatment Effects by Stage

Metagenomic functional profiling revealed mostly small, stage-specific pathway responses, with the most significant treatment effects observed at V4.

At V2, pathway metrics showed mixed responses with high variability, reflecting dynamic changes to the microbiome in response to treatment during the early establishment phase. Calcium transport potential increased (+8.7 percentile points), while nitrogen fixation showed modest enhancement (+2.7 percentile points). Community structure metrics at V2 showed diversity increase (+6.0%) and evenness increase (+26.7%), though neither reached statistical significance. Mycorrhizae populations showed a marginally significant reduction in treated areas (-24 percentile points, $p<0.10$) that persisted throughout the growing season, though mycorrhizae populations in treated areas rebounded somewhat by V7.

By V4, several functional pathways showed statistically significant or marginally significant treatment effects. Nitrification potential showed a statistically significant increase (+1.7 percentile points, $p = 0.03$) in a system with very low

nitrification potential to begin with (normalized scores less than the 10th percentile, see Section 6), representing a potential to improve nitrate availability for plant uptake. Iron acquisition potential showed significant enhancement (+5.5 percentile points, p = 0.04), indicating modest improvement in microbial iron-solubilizing capacity. Sulfur reduction potential decreased significantly (-26.6 percentile points, p = 0.04), suggesting asuppresed sulfur cycling dynamics, as sulfur oxidation potential also showed a non-significant decrease in treated areas. Microbial diversity and evenness scores were higher in treated areas with marginal significance, indicating persisting changes to the microbial community in response to treatment at V4.

At V7, the most significant pathway response was observed for phosphorus solubilization potential, which increased +14.4 percentile points (p = 0.006), indicating enhanced microbial P-cycling potential during the transition toward reproductive growth. Community structure showed modest increases in diversity (+6.3%), though high variability limited statistical significance. Mycorrhizal populations remained suppressed in treated roots at V7, continuing the trend from V2 and V4, though the changes were not statistically significant. The V7 pathway reponses suggest continued microbial functional responses extending into late vegetative growth though generally smaller in magnitude, including both beneficial and potentially detrimental changes.

Table 3.1: Microbial Functional Pathway Changes by Growth Stage

Pathway	V2 Change	V4 Change	V7 Change
Nitrification	+9.00	+1.7*	-2.1
P Solubilization	+4.83	+0.08	+14.4*
Iron Acquisition	-0.10	+5.6*	+1.9
Sulfur Reduction	-5.1	-26.6*	+7.0
N Fixation	+2.7	-10.5	-11.4
Org C Breakdown	-2.7	+5.9	-4.2

*Note: * p < 0.05. Values represent percentile point change in pathway potential.*

4. PLANT TISSUE EFFECTS

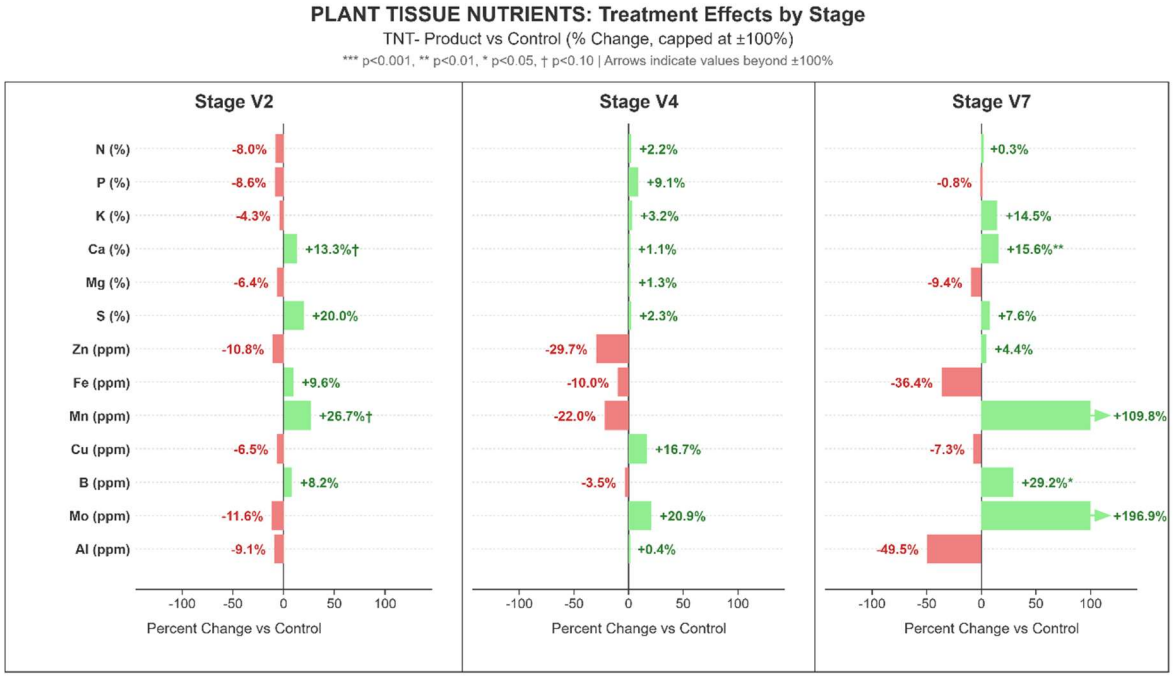

Figure 3. Plant Tissue Nutrient Effects - Treatment Response

Plant tissue nutrient data revealed mixed treatment responses across growth stages, with tissue macronutrient levels generally stable, and the most statistically significant finding being enhanced calcium levels in treated plants at V7.

At V2, tissue nutrients showed variable responses: sulfur increased (+20.0%), calcium increased modestly (+13.3%), while nitrogen (-8.0%), phosphorus (-8.6%), and potassium (-4.3%) showed slight reductions. Iron showed modest increase (+9.6%).

By V4, tissue nutrient responses moderated, with most nutrients within 10% of control levels. Phosphorus showed a positive trend (+9.1%), while potassium (+3.2%), nitrogen (+2.2%), and sulfur (+2.3%) remained near control levels. Calcium showed minimal change (+1.1%). Iron declined (-10.0%) and zinc showed the largest reduction (-29.7%), though neither reached statistical significance.

At V7, the significant tissue calcium increase (+15.6%, $p = 0.014$) represents the clearest plant nutritional benefit in this trial. This finding aligns with the elevated soil calcium observed at V4 (+39.2%, $p = 0.008$), providing evidence for successful soil to plant nutrient transfer. Potassium levels showed a positive trend in treated tissues (+14.5%), nitrogen remained stable (+0.3%), and phosphorus

was essentially unchanged (-0.8%). Manganese (+109.8%, p = 0.375) and molybdenum (+196.9%) showed substantial elevation in treated plants but variability limited statistical power, while iron (-36.4%) and aluminum (-49.5%) saw large but non-significant declines compared to control levels.

Table 4.1: Plant Tissue Nutrient Changes by Growth Stage

Nutrient	Units	V2 Change	V4 Change	V7 Change	V7 p
Calcium	% Ca	+13.3%	+1.1%	+15.6%	0.014*
Nitrogen	% N	-8.0%	+2.2%	+0.3%	0.955
Phosphorus	% P	-8.6%	+9.1%	-0.8%	0.960
Potassium	% K	-4.3%	+3.2%	+14.5%	0.181
Sulfur	% S	+20.0%	+2.3%	+7.6%	0.405
Iron	ppm Fe	+9.6%	-10.0%	-36.4%	0.491

*Note: * p < 0.05. Values represent percent change from control.*

5. CARBON CYCLING AND SOIL HEALTH

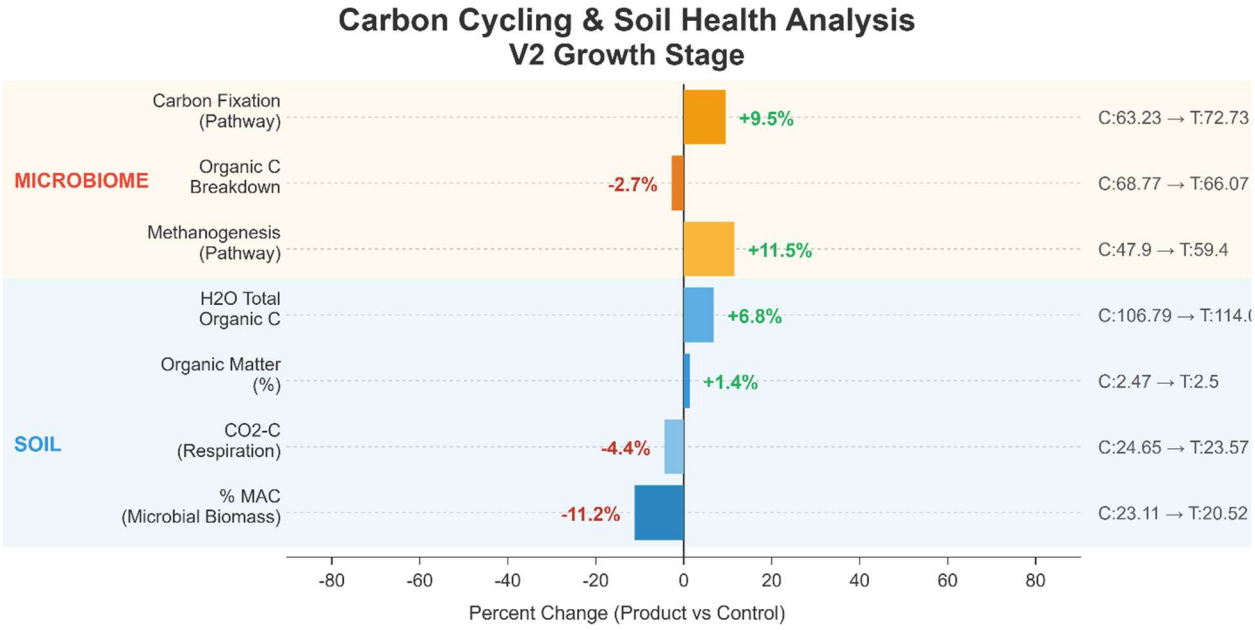

Figure 4. Carbon Cycling and Soil Health Metrics at V2 Growth Stage

Carbon cycling analysis revealed varying patterns across the growing season, with organic matter showing a pronounced late-season response. At V2, CO2-C respiration and percent microbially active carbon (% MAC) showed modest decreases (-4.4% and -11.2%, respectively), while organic matter remained relatively stable (+1.4%) and total Water-extractable organic carbon was slightly elevated in treated soils. Organic carbon breakdown potential showed a slight decrease (-2.7 percentile points), while carbon fixation potential varied highly across replicates.

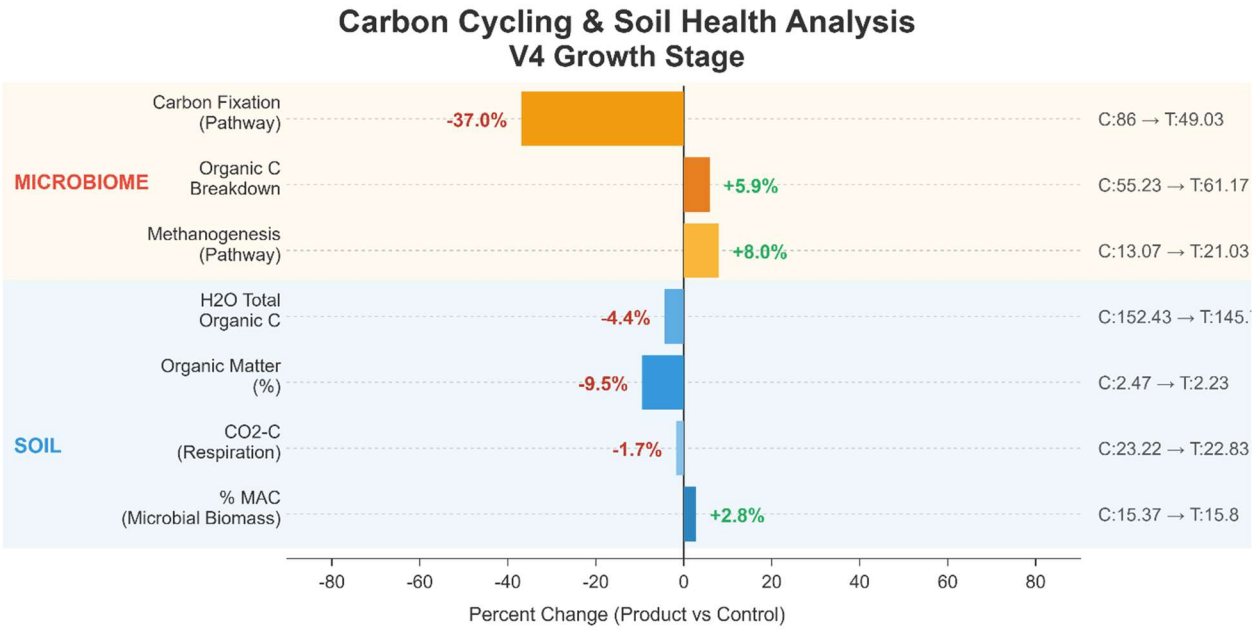

Figure 5. Carbon Cycling and Soil Health Metrics at V4 Growth Stage

By V4, soil respiration (CO2-C) remained near control levels (-1.7%), indicating relatively stable microbial metabolic function. Carbon fixation potential showed a large but non-signifcant decrease in treated areas at V4, indicating some level of disruption in carbon cycling. However, slight elevation of organic carboon breakdown potential may be acting to offset the losses in carbon fixtion potential, as soil carbon levels and microbial biomass remained relatively stable. The correlation analysis revealed that organic carbon breakdown showed strong inverse correlation with community diversity (r = -0.929, p = 0.0003), suggesting that active carbon decomposition occurs through community specialization.

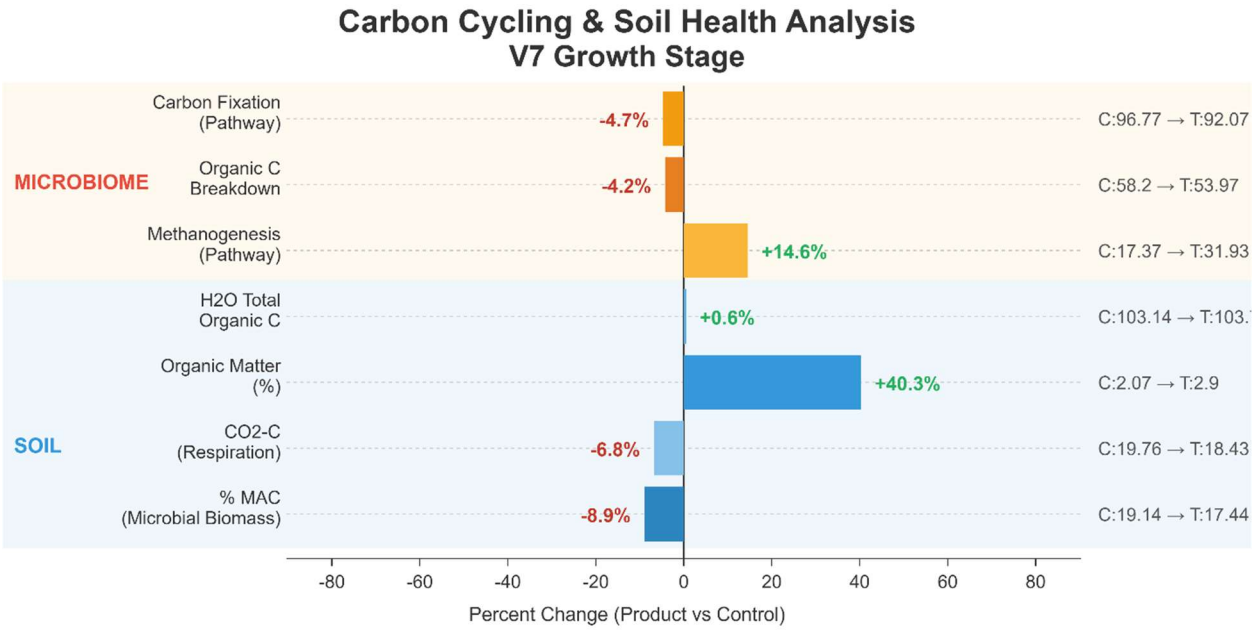

Figure 6. Carbon Cycling and Soil Health Metrics at V7 Growth Stage

At V7, organic matter showed the strongest average treatment effect (+40.3% above control), as %OM in treated areas actually increased from V4 to V7 (2.23% to 2.9%), while OM was consumed in treated areas (2.47% to 2.07%), though the high variability in OM between sampling locations limits the strength of these effects. Soil respiration (CO2-C) declined modestly (-6.8%), which may reflect the community specialization patterns identified in correlation analysis rather than reduced microbial function. The inverse correlation between soil sulfur and organic carbon breakdown potential ($r = -0.934$, $p = 0.0002$) suggests that carbon cycling potential may be consuming or competing with sulfur pools.

6. NITROGEN CYCLING

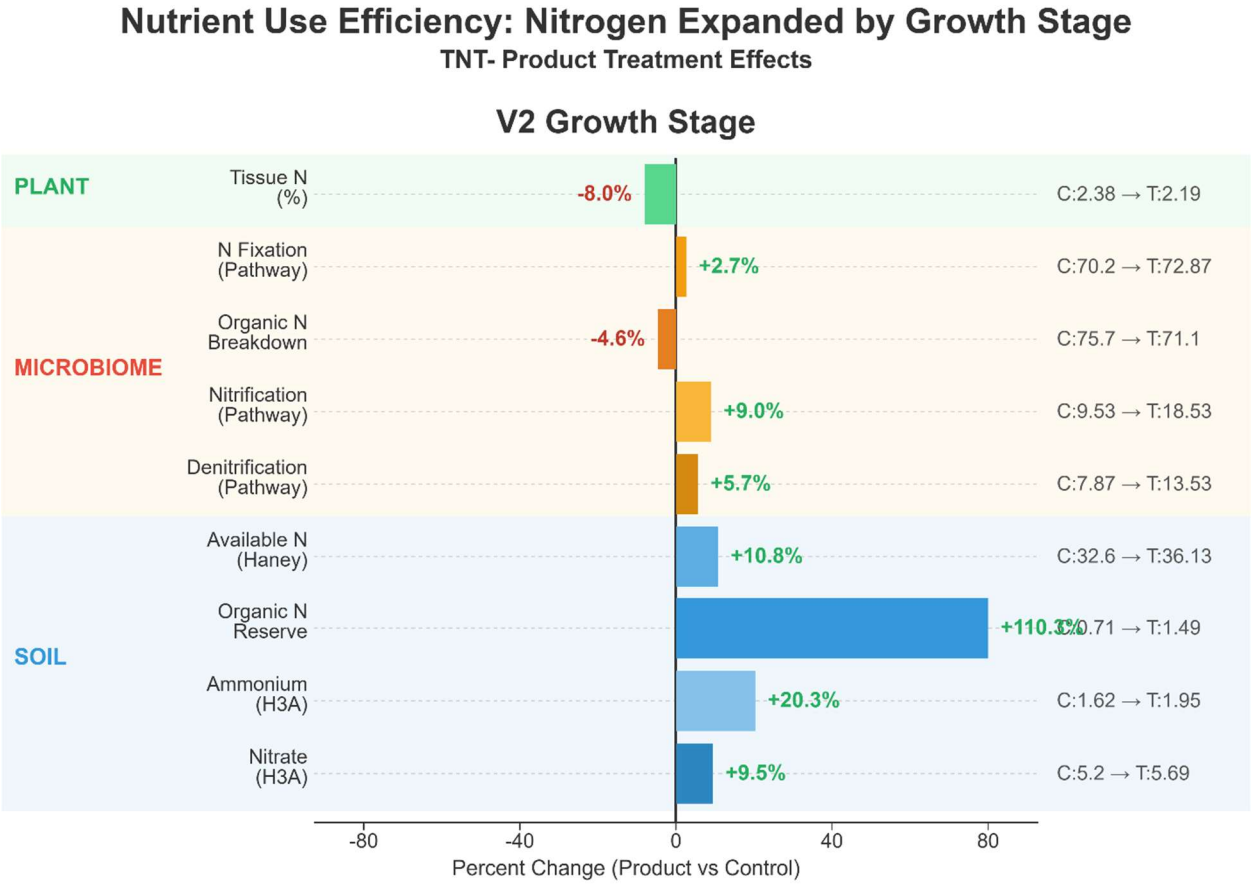

Figure 7. Nitrogen Cycling Dynamics at V2 Stage

At V2, nitrogen cycling showed mixed initial patterns. Soil available nitrogen increased modestly (+10.8%). Organic N reserve increased substantially (+110.3%), though high variability limited statistical significance ($p = 0.345$). Nitrogen fixation potential showed positive response (+2.7 percentile points), and nitrification potential increased (+9.0 percentile points). Tissue nitrogen showed a slight decrease (-8.0%), potentially reflecting the effects of early establishment dynamics in the microbiome on nutrient uptake into plant tissues. The substantial increase in organic N reserve suggests treatment may enhance nitrogen retention in organic pools.

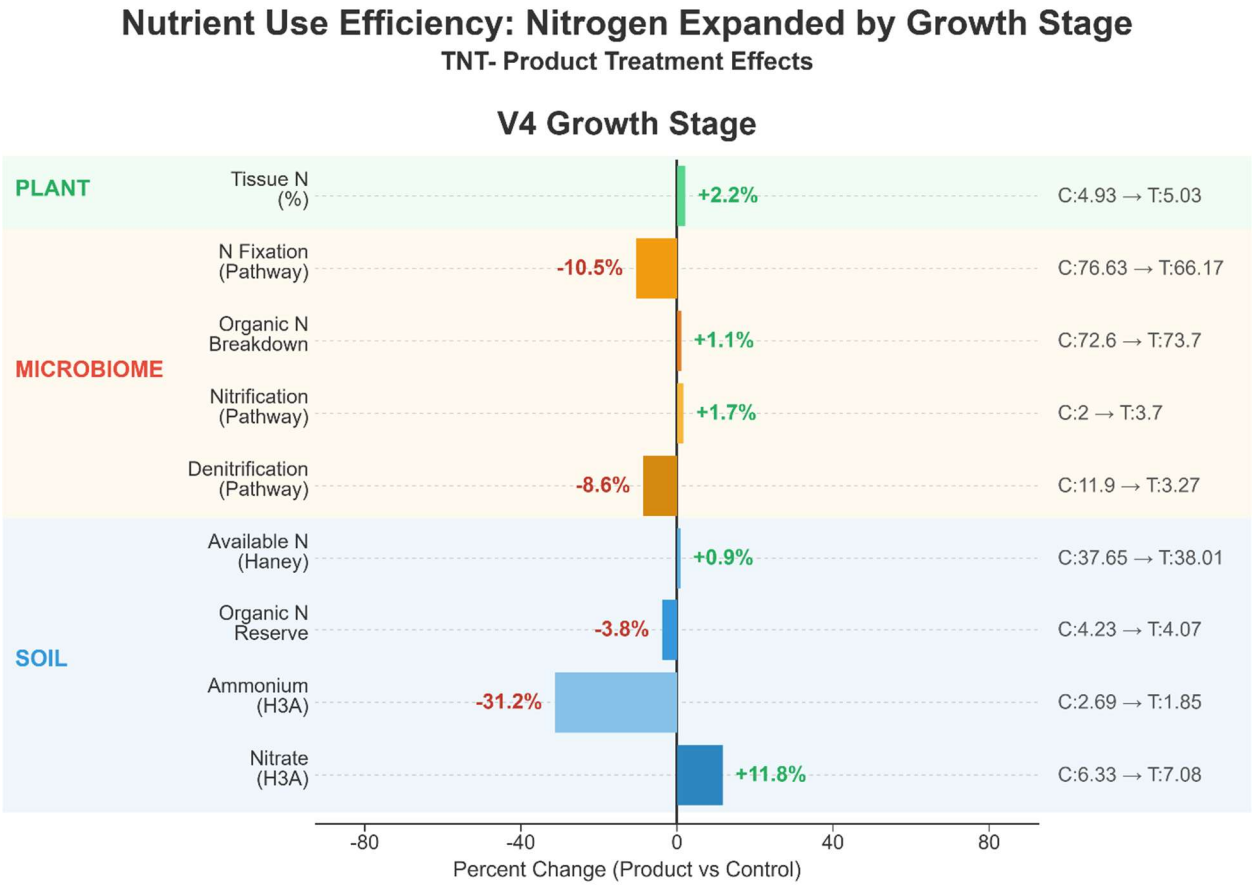

Figure 8. Nitrogen Cycling Dynamics at V4 Stage

By V4, nitrogen cycling reached functional stability with key pathway enhancement. Available nitrogen remained near control levels (+0.9%), while nitrification potential increased significantly (+1.7 percentile points, p = 0.045). Nitrogen fixation potential showed minimal change (-10.5 percentile points), and tissue nitrogen increased modestly (+2.2%). A statistically significant increase in nitrification potential was observed at V4; however, the magnitude of the shift was modest (+1.7 percentile points), indicating a subtle but detectable treatment effect during mid-vegetative growth.

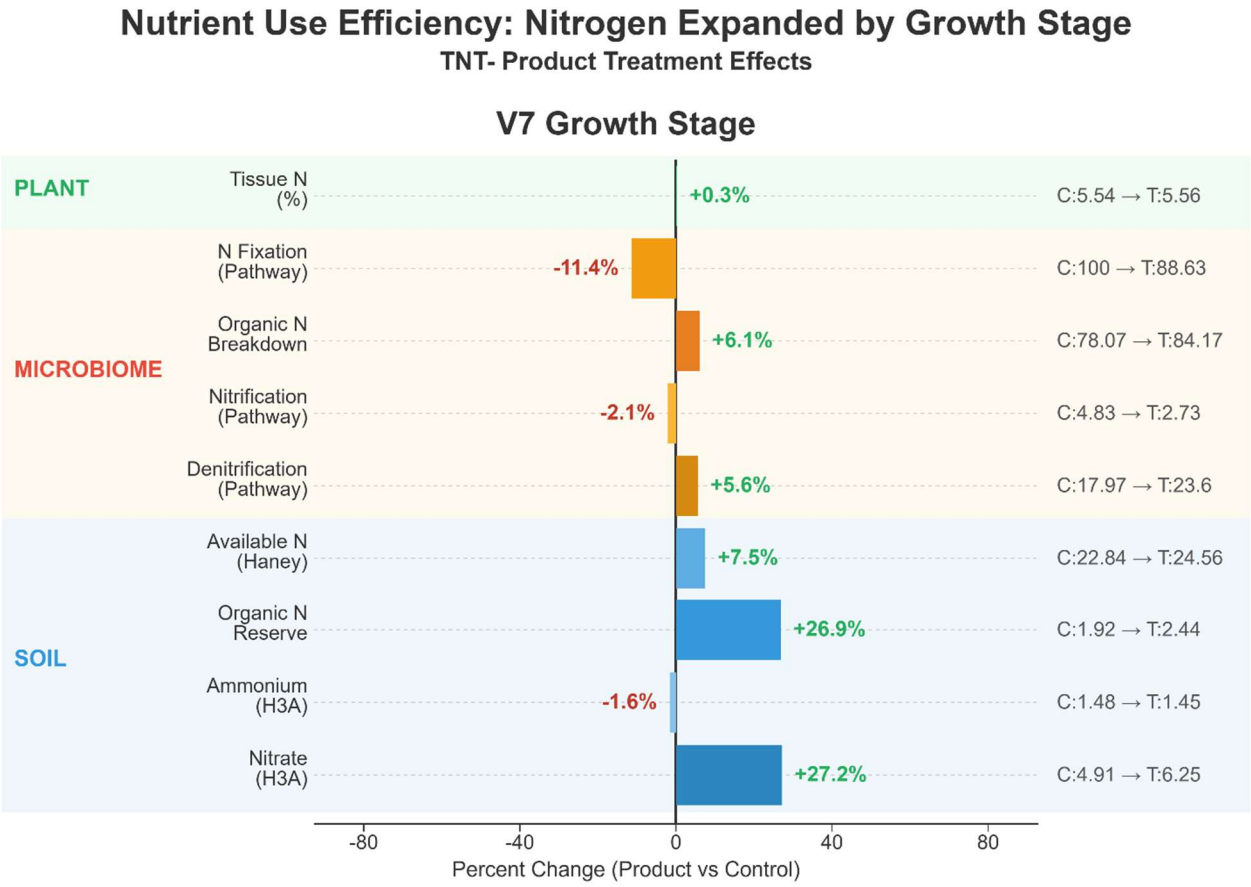

Figure 9. Nitrogen Cycling Dynamics at V7 Stage

At V7, nitrogen dynamics showed continued stability. Available nitrogen increased (+7.5%) relative to the control. Organic N reserve maintained elevation (+26.9%). Nitrogen fixation potential declined (-11.4 percentile points), while nitrification returned to control levels (-2.1 percentile points). Tissue nitrogen remained stable (+0.3%). The late-season inorganic nitrogen increase suggests continued mineralization from enhanced organic nitrogen pools established earlier in the season.

General Nitrogen Summary

Nitrogen cycling demonstrated consistent organic nitrogen reserve enhancement across stages (+110.3% at V2, +26.9% at V7), with statistically significant mid-season nitrification potential enhancement (+1.7 percentile points, $p = 0.045$ at V4). Organic nitrogen breakdown correlated strongly with tissue nitrogen ($r = 0.829$, $p = 0.006$), consistent with mineralization contributing to plant nitrogen nutrition. In contrast, *Bradyrhizobium* relative abundance declined (-61.4%) in

response to treatment, which may reflect reduced nodulation demand under higher mineral N availability, compositional shifts in the rhizosphere community, or compartment/timing effects rather than a definitive loss of fixation capacity, as nitrogen fixation potential remained generally high (70th percentile or higher).

7. PHOSPHORUS CYCLING

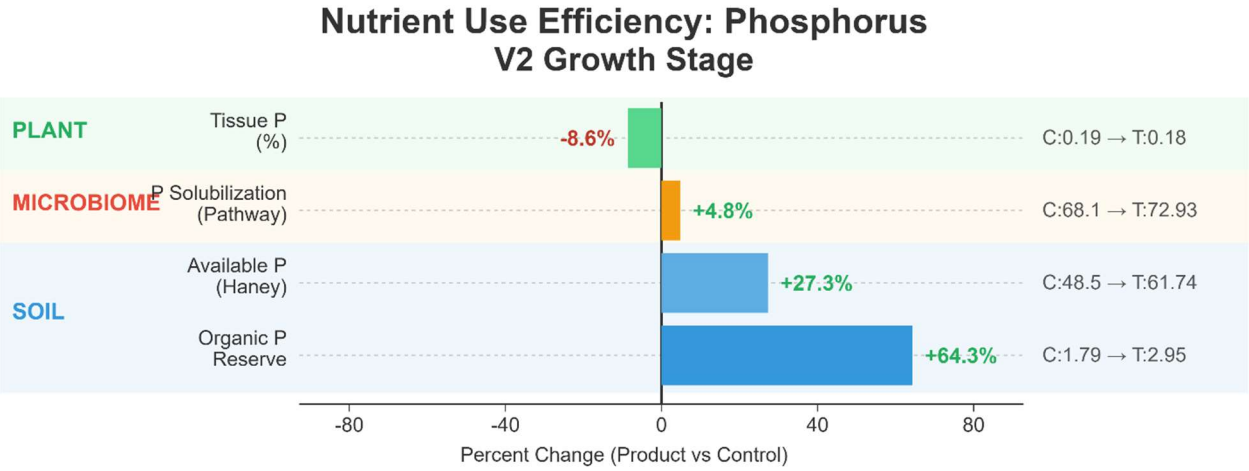

Figure 10. Phosphorus Cycling Dynamics at V2 Stage

At V2, phosphorus cycling showed elevated soil pools without significantly enhanced P slubilization potential. Available phosphorus showed enhancement (+27.3%), though non-significant. Organic P reserve increased substantially (+64.3%), suggesting treatment may have enhanced phosphorus retention in organic fractions. Phosphorus solubilization potential showed modest increase (+4.8 percentile points). Tissue phosphorus decreased slightly (-8.6%), potentially reflecting limitations posed by reduced mycorrhizal populations, or dilution during rapid early growth rather than supply limitation.

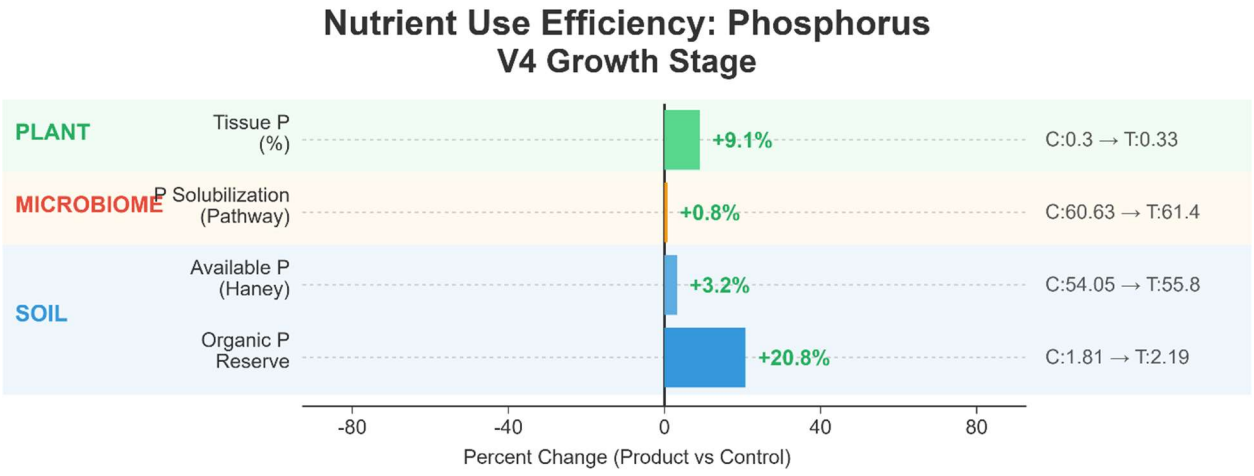

Figure 11. Phosphorus Cycling Dynamics at V4 Stage

By V4, phosphorus dynamics showed stability across soil, pathway, and tissue compartments. Available phosphorus showed minimal change (+3.2%). Organic P reserve maintained enhancement (+20.8%). Phosphorus solubilization potential remained near control levels (+0.80 percentile points). Tissue phosphorus showed positive trend (+9.1%), suggesting improved phosphorus uptake efficiency despite stable soil and pathway metrics.

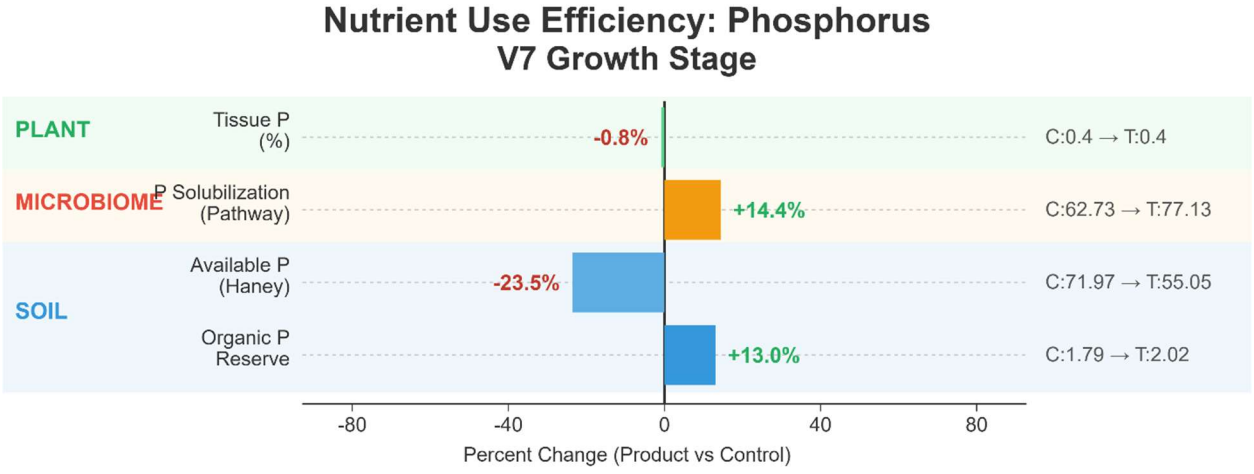

Figure 12. Phosphorus Cycling Dynamics at V7 Stage

At V7, phosphorus solubilization potential reached statistical significance (+14.0 percentile points, p = 0.013). This late-season pathway enhancement indicates improved microbial P-cycling potential during the transition toward reproductive

growth. H3A total phosphorus declined (-23.5%), potentially reflecting uptake from soil pools. Tissue phosphorus remained stable (-0.8%). The significant late-season pathway enhancement suggests continued microbial P-cycling benefits.

General Phosphorus Summary

Phosphorus cycling demonstrated early-season soil pool enhancement (+30.2% total P at V2) followed by significant late-season pathway enhancement (+14.0 percentile points P solubilization, p = 0.013 at V7). Effects on tissue phosphorus concentrations were minimal, and all samples remained above sufficiency levels. The correlation analysis identified that phosphorus solubilization potential showed strong coordination with potassium solubilization potential (r = +0.974, p < 0.0001), consistent with shared organic acid production by both pathways. Community evenness showed negative correlation with tissue phosphorus (r = -0.777, p = 0.014), suggesting that specialized communities may better support phosphorus nutrition. The mycorrhizal decline (-25.4%) observed in taxonomic analysis may partially offset pathway benefits for phosphorus acquisition.

8. POTASSIUM CYCLING

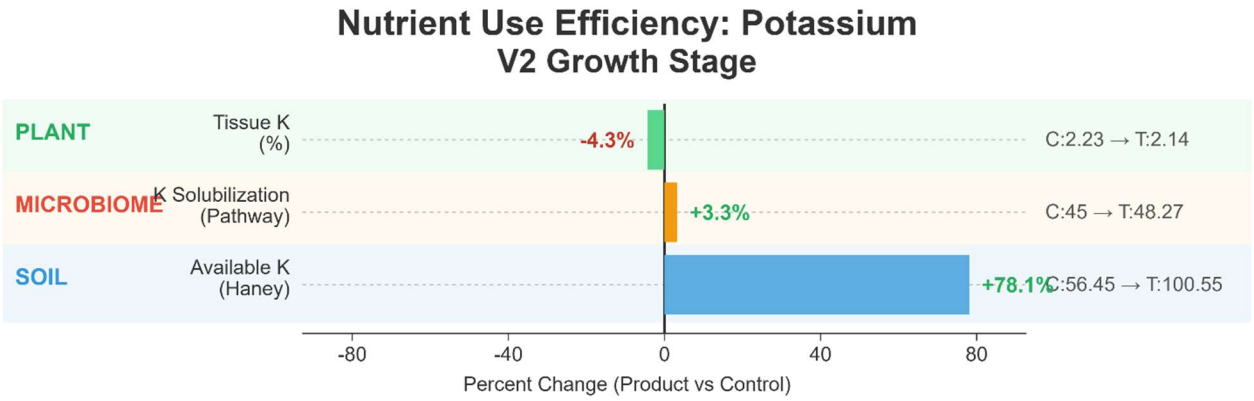

Figure 13. Potassium Cycling Dynamics at V2 Stage

At V2, potassium cycling exhibited a soil mobilization response. Available potassium increased substantially (+78.1%, p = 0.052). This consistent early-season potassium mobilization represents one of the more notable treatment effects in this trial. Potassium solubilization potential showed modest increase (+3.3 percentile points). Tissue potassium showed slight decrease (-4.3%), suggesting that enhanced soil availability did not immediately translate to tissue concentration, possibly due to dilution during rapid early growth.

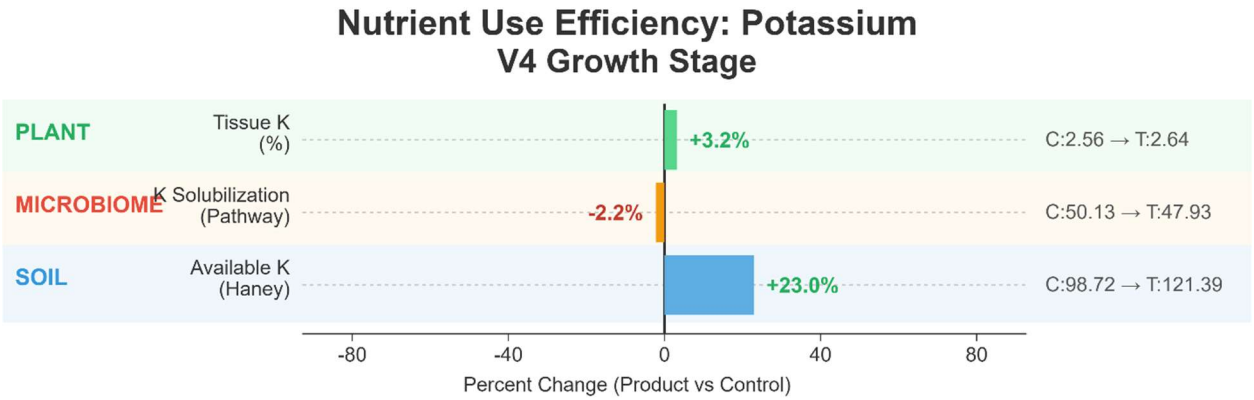

Figure 14. Potassium Cycling Dynamics at V4 Stage

By V4, potassium enhancement persisted at reduced magnitude. Available potassium showed consistent enhancement (+23.0%, p = 0.073). Potassium solubilization potential remained at control levels (-2.2 percentile points). Tissue potassium showed minimal change (+3.2%). The sustained but diminishing potassium effect suggests that treatment provides early-season mobilization benefits that moderate through mid-vegetative growth.

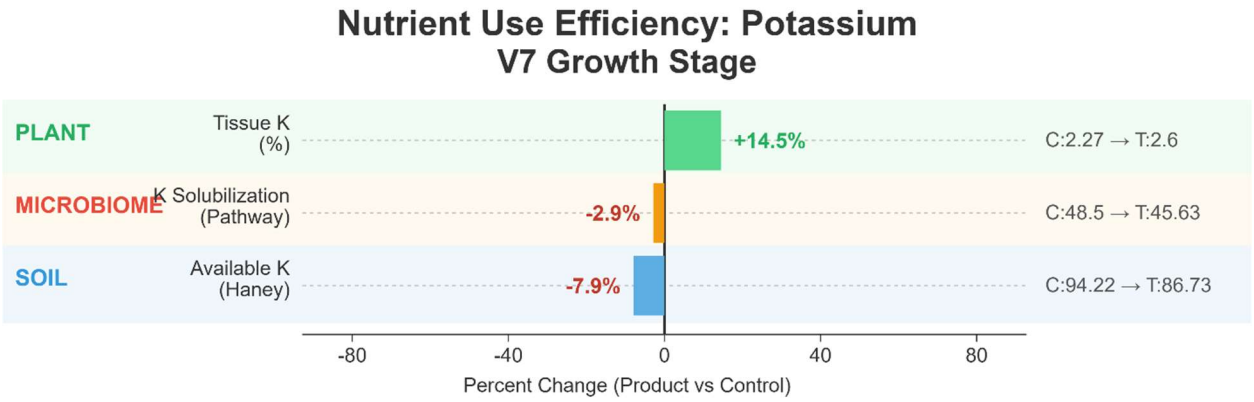

Figure 15. Potassium Cycling Dynamics at V7 Stage

At V7, potassium dynamics showed equilibration. Available potassium returned to near-control levels (-7.9%). Potassium solubilization potential remained stable (-2.9 percentile points). Tissue potassium showed positive trend (+14.5%), suggesting that earlier soil pool enhancement may support late-season plant uptake. The correlation analysis identified that potassium solubilization potential showed strong inverse relationship with diversity (r = -0.885, p = 0.0015), indicating that K mobilization occurs through specialized microbial communities.

General Potassium Summary

Soil potassium levels demonstrated consistent early-season soil enhancement in treated areas (+78.1% at V2, +23.0% at V4), with effects diminishing by V7 (-7.9%). This temporal pattern suggests treatment may provide transient early-season K mobilization rather than long-term establishment of colonies of potassium solubilizing bacteria. Tissue potassium showed progressive improvement from -4.3% at V2 to +14.5% at V7, suggesting delayed translation of soil availability to plant uptake. The correlation between soil potassium and tissue nitrogen identified in preliminary analysis ($r = +0.836$, $p = 0.038$) suggests functional linkages between potassium availability and nitrogen metabolism.

9. SULFUR CYCLING

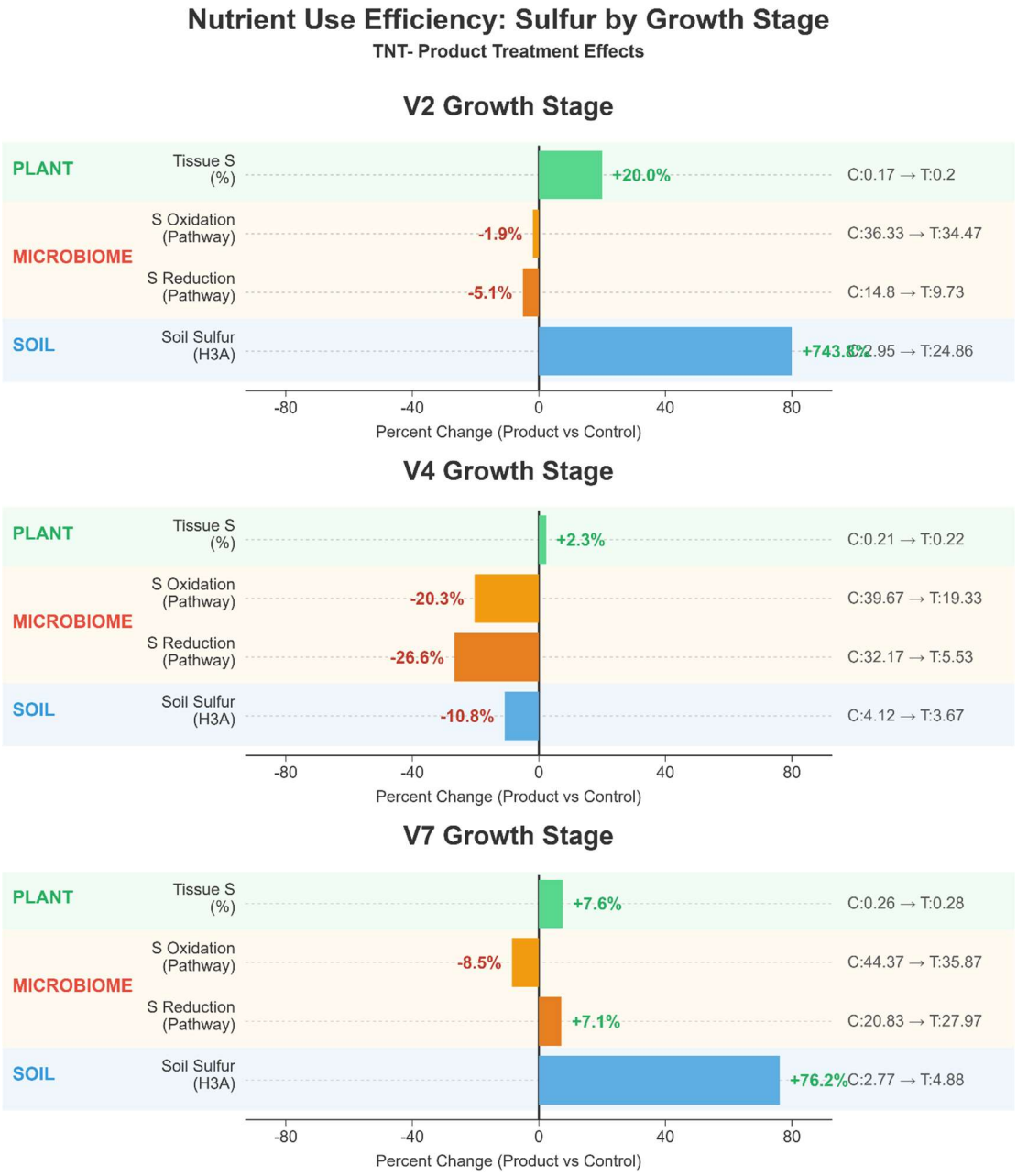

Figure 16. Sulfur Cycling Dynamics Across Growth Stages

At V2, soil H3A ICAP sulfur showed a substantial but highly variable increase in treated areas (+743.8%, p = 0.366), reflecting one treated replicate with exceptionally high sulfur. Sulfur oxidation potential decreased modestly (-1.9

percentile points) and sulfur reduction potential declined (-5.1 percentile points). Tissue sulfur increased (+20.0%), indicating enhanced plant sulfur status despite pathway reductions.

By V4, sulfur reduction potential in treated areas showed marginally a signifcant decrease (-26.6 percentile points, p = 0.053), soil sulfur declined (-10.8%), and sulfur oxidation potential decreased (-20.3 percentile points), suggesting substantially altered sulfur cycling dynamics. Tissue sulfur remained near control levels (+2.3%). The correlation analysis revealed that sulfur oxidation potential showed exceptionally strong inverse correlation with diversity (r = -0.984, p < 0.0001), the strongest cross-domain relationship identified in this analysis, indicating that sulfur-cycling specialists may reduce overall community diversity when active.

At V7, soil sulfur increased (+76.2%), while sulfur reduction potential showed slight increase (+7.6 percentile points) and sulfur oxidation decreased (-8. percentile points). Tissue sulfur remained elevated (+7.6%). The integrated pattern suggests that treatment modulates sulfur cycling dynamics, potentially shifting between oxidation and reduction states depending on soil conditions. The strong inverse correlation between soil sulfur and multiple pathways (organic carbon breakdown potential: r = -0.934; sulfur reduction potential: r = -0.922) suggests that sulfur availability may constrain certain microbial functional responses.

10. CALCIUM CYCLING

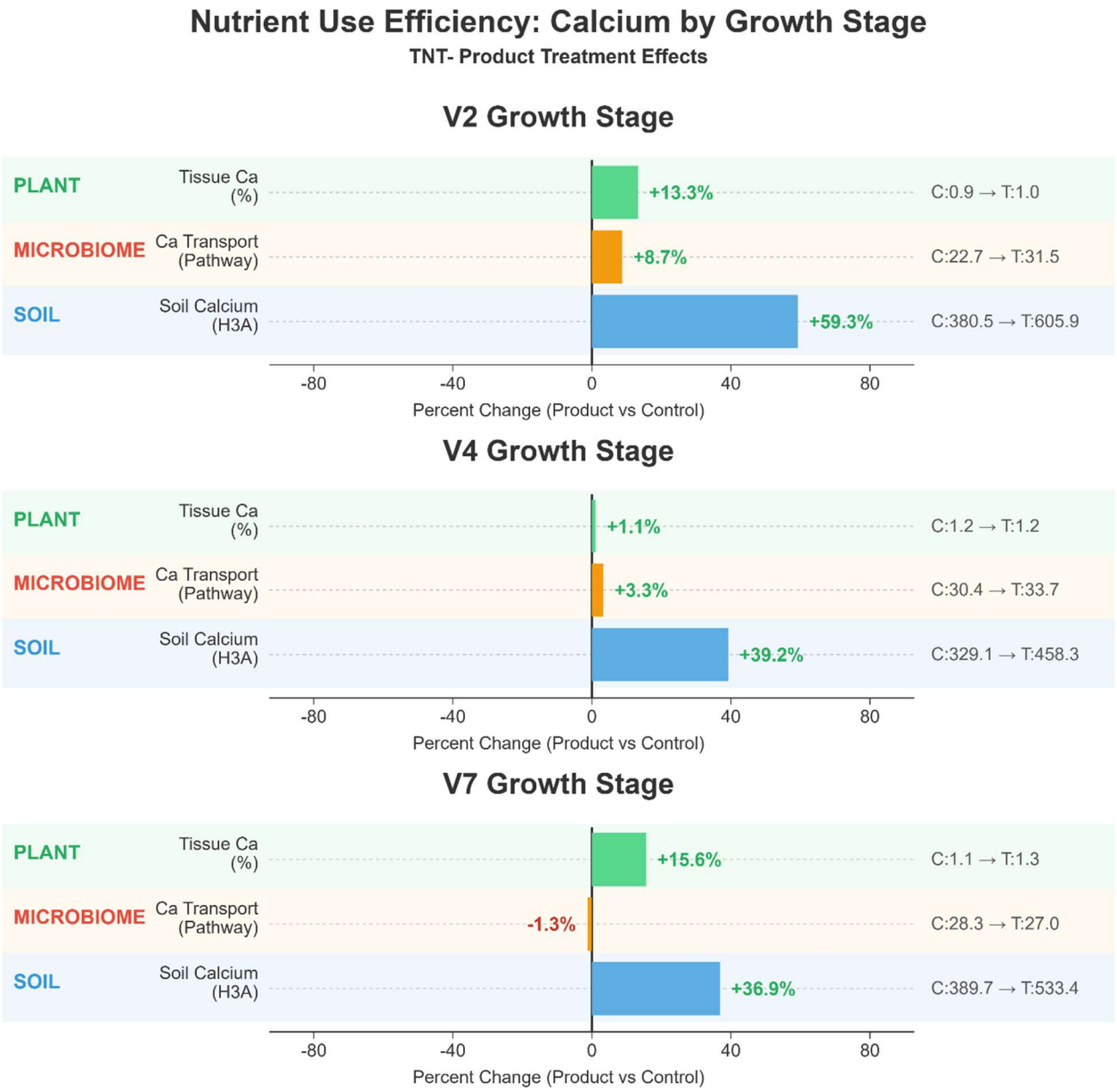

Figure 17. Calcium Cycling Dynamics Across Growth Stages

Calcium cycling demonstrated clear soil to plant nutrient transfer benefit, with slight enhancement of microbial cycling potential that attenuated throughout the season. At V2, H3A ICAP calcium increased substantially (+59.3%, p = 0.106), while calcium transport potential showed modest enhancement (+8.7 percentile

points).Tissue calcium showed positive response (+13.3%, p = 0.143),indicating early treatment benefits for calcium nutrition.

By V4, the soil calcium enhancement reached statistical significance (+39.2%, p = 0.008),representing the most robust soil chemistry finding in this trial. Calcium transport potential remained near control levels (+3.3 percentile points).This significant soil calcium increase provides the mechanistic basis for downstream tissue benefits. The correlation analysis showed that soil calcium correlated positively with community evenness (r = +0.879, p = 0.0018),suggesting calcium-rich conditions support balanced microbial communities.

At V7, elevated tissue calcium in treated areas reached statistical significance (+15.6%, p = 0.014),while soil calcium remained elevated (+36.9%).In contrast, calcium transport pathway potential showed minimal change (-1.3 percentile points),suggesting the tissue response was driven primarily by improved calcium availability and plant-mediated uptake dynamics (e.g., mass flow/transpiration and root physiology)rather than an expansion in microbial calcium transporter gene abundance. This late-season tissue calcium enhancement represents one of the primary nutritional gains observed in this trial and may help to support pod and seed development in soybean crops.

11. IRON CYCLING

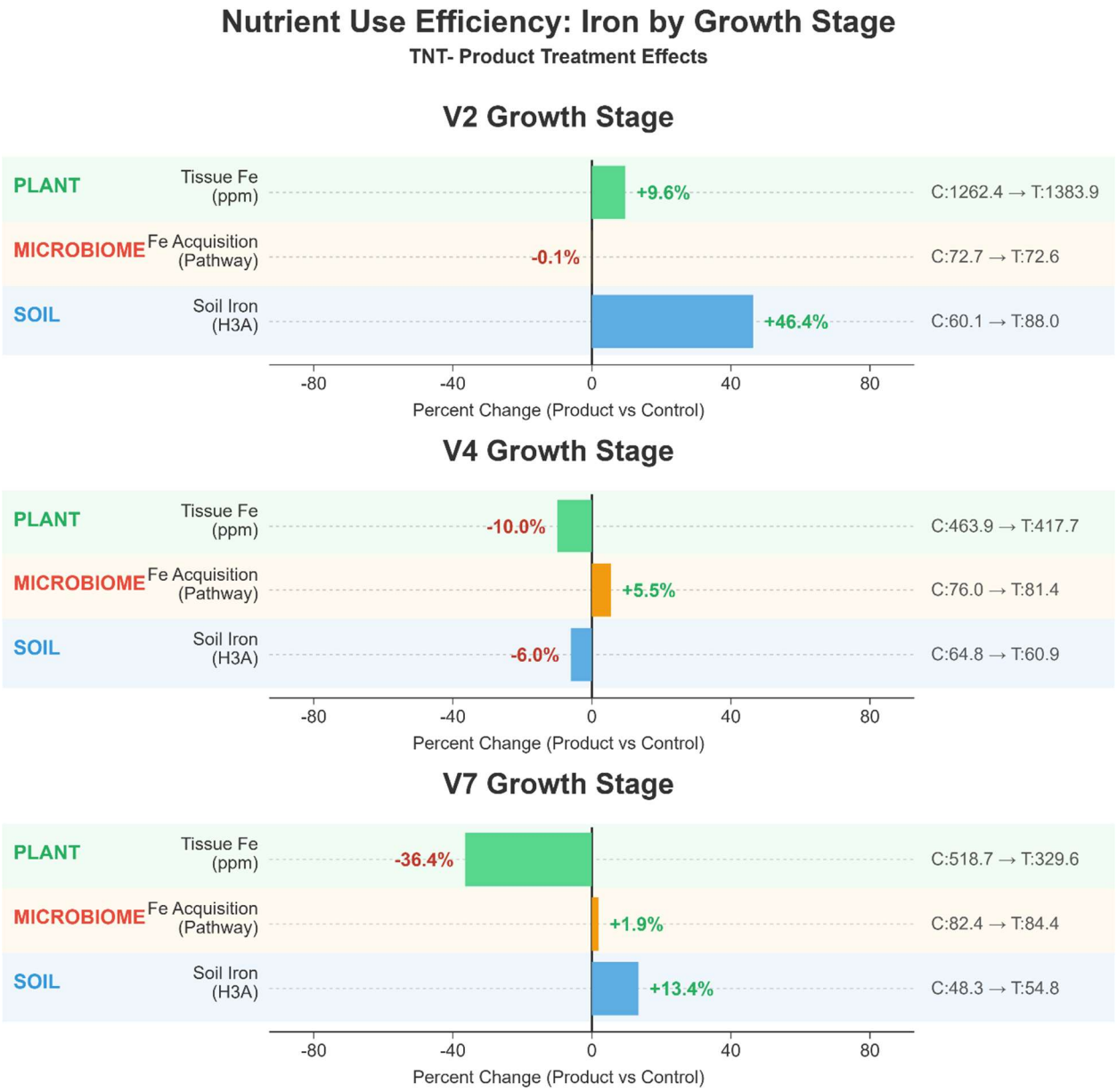

Figure 18. Iron Cycling Dynamics Across Growth Stages

Iron cycling exhibited variable patterns across growth stages. At V2, soil H3A ICAP iron increased (+46.4%), while iron acquisition potential showed minimal change (-0.10 percentile points). Tissue iron increased modestly (+9.6%), indicating adequate iron nutrition during early establishment.

By V4, iron acquisition potential showed marginal enhancement (+5.5 percentile points, p = 0.056),indicating modest improvement in microbial siderophore production capacity. Soil iron declined slightly (-6.0%),while tissue iron decreased (-10.0%).The correlation analysis identified that iron acquisition potential showed positive correlation with community evenness (r = +0.841, p = 0.0045),representing a departure from the dominant pattern of inverse pathway-diversity relationships observed for other nutrients, aside from soil calcium, which also increased with an increase in community evenness.

At V7, soil iron increased (+13.4%),and iron acquisition potential showed slight enhancement (+1.9 percentile points).Tissue iron showed the largest decline (-36.4%, p = 0.491),though high variability limited statistical significance. The positive correlation between iron acquisition potential and evenness suggests that siderophore-producing communities maintain greater balance, possibly because iron acquisition involves diverse microbial strategies rather than a single dominant population.

12. NUTRIENT UPTAKE SUMMARY

V2 represented an early establishment phase with disruptions to overall microbial activity (reduced %MAC and CO2-C) in exchange for increased microbial diversity and evenness, and notable potassium mobilization effects. The significant soil potassium enhancement occurred without proportional tissue increase, suggesting mobilization from mineral reserves preceded plant uptake. Calcium showed coordinated soil and tissue increases in response to treatment. Tissue sulfur increased despite pathway reductions, suggesting alternative sulfur supply mechanisms.

V4 demonstrated key functional pathway shifts with significant treatment effects. Nitrification potential was substantially increased in treated areas at V4 (although it remained low overall), potentially contributing to elevated nitrate in treated soils at all growth stages. Elevated soil calcium in treated areas reached peak statistical significance at V4. Iron acquisition potential showed marginal enhancement, while sulfur reduction potential declined. These mid-season pathway responses indicate functional community differentiation.

V7 showed translation of earlier soil benefits to plant tissue outcomes. The significant increase in tissue calcium in treated areas confirmed successful soil to plant transfer. Phosphorus solubilization potential reached significance, indicating enhanced late-season P-cycling capacity. Tissue potassium showed a positive trend, suggesting delayed uptake benefits.

Overall, the data suggests that the response to treatment with TNT HEF 2-3-0 exhibited a phase response pattern: early-season microbiome restructuring and potassium mobilization (V2), mid-season functional pathway enhancement and soil nutrient stability (V4), and late-season plant nutritional benefits (V7). The calcium pathway showed the clearest benefit progression, from significant soil enhancement at V4 to significant tissue increase at V7. Phosphorus showed delayed pathway benefits while nitrogen showed consistent organic reserve enhancement. The correlation analysis revealed that select functional pathway enhancements appear to occur through community specialization rather than diversification, as indicated by strong inverse relationships between pathway potential and diversity metrics.

13. TAXONOMY SUMMARY

Taxonomic analysis of the rhizosphere bacterial and fungal communities revealed substantial treatment-induced restructuring, with distinct functional implications for soybean production. Analysis included shotgun metagenomic sequencing with characterization of the top 20 bacterial and fungal genera across all growth stages.

Bacterial Community Response

The bacterial community showed mixed responses to TNT HEF 2-3-0. Notable increases were observed in nutrient cycling genera: *Serratia* increased from 0.13% to 0.89% community abundance (+595.6%), *Enterobacter* increased from 0.20% to 1.41% (+590.8%), *Paraburkholderia* increased from 0.90% to 2.13% (+135.2%), and *Rhodococcus* increased from 1.81% to 3.13% (+73.1%). The bacterial biocontrol guild increased overall (+15.3%), and the nutrient cycling guild showed substantial enhancement (+32.6%).

The most significant bacterial concern was the decline in nitrogen-fixing genera. *Bradyrhizobium*, the primary soybean nitrogen-fixing symbiont, declined substantially from 26.75% to 10.33% (-61.4%). This reduction drove an overall 47.6% decline in the nitrogen fixation guild, representing a potential constraint on biological nitrogen fixation capacity. Additional genera showing decline included *Leifsonia* (-35.6%), *Pseudonocardia* (-100.0%), *Delftia* (-100.0%), and *Phycicoccus* (-100.0%).

Table 13.1: Notable Bacterial Genera Changes

Genus	Untreated	Treated	% Change	Function
Serratia	0.13%	0.89%	+595.6%	Nutrient cycling
Enterobacter	0.20%	1.41%	+590.8%	Nutrient cycling
Paraburkholderia	0.90%	2.13%	+135.2%	N-fixation/biocontrol
Rhodococcus	1.81%	3.13%	+73.1%	Organic degradation
Bradyrhizobium	26.75%	10.33%	-61.4%	N-fixation (primary)

Fungal Community Response

The fungal community showed increases in biocontrol genera alongside potential pathogen increases. *Trichoderma*, a well-characterized biocontrol organism, increased substantially (+129.5%),contributing to an overall fungal biocontrol guild increase of +125.1%. Other genera showing increase included *Furcasterigmium* (+369.0%),*Epicoccum* (+146.5%),*Cladosporium* (+115.5%),and *Acremonium* (+106.7%).The saprophyte guild increased +36.6%, potentially supporting organic matter decomposition.

Mycorrhizal fungi showed overall decline (-25.4%),with *Gigaspora* and related arbuscular mycorrhizal genera decreasing in relative abundance. This decline may affect phosphorus acquisition capacity, particularly in soils with limited phosphorus availability. The potential pathogen guild increased (+41.8%).

Table 13.2: Fungal Functional Guild Changes

Guild	% Change	Assessment
Biocontrol	+125.1%	Major increase
Saprophytes	+36.6%	Moderate increase
Potential Pathogens	+41.8%	Monitor
Mycorrhizal	-25.4%	Decline

14. PATHOGEN ANALYSIS

Pathogen analysis revealed time-dependent treatment effects, with strong early-season suppression followed by late-season equilibration. Total pathogen occurrence decreased by 13.2% across all timepoints (174 untreated to 151 treated occurrences). The temporal pattern showed distinct phases: V2 (-42.4%), V4 (-46.2%), and V7 (+8.8%).

Table 14.1: Pathogen Pressure by Growth Stage

Growth Stage	Untreated (avg)	Treated (avg)	% Change	Assessment
V2 (Early)	11.0	6.3	-42.4%	Favorable
V4 (Mid)	13.0	7.0	-46.2%	Favorable
V7 (Late)	34.0	37.0	+8.8%	Monitor
TOTAL	174	151	-13.2%	Net favorable

Pathogens Suppressed

Complete suppression (100% reduction) was achieved for several economically important soybean pathogens: brown spot/*Septoria* leaf spot (2 to 0), *Diaporthe* seed decay (3 to 0), and stem canker (*Diaporthe* spp., 3 to 0). Substantial reductions were observed for soybean cyst nematode (-75.0%), *Verticillium* wilt (-75.0%), *Microdochium* patch (-66.7%), red crown rot (-50.0%), bacterial canker (-50.0%), sudden death syndrome (-50.0%), and charcoal rot (*Macrophomina phaseolina*, -50.0%).

Table 14.2: Top Pathogens Suppressed

Disease	Untreated	Treated	% Change
Brown Spot/Septoria Leaf Spot	2	0	-100.0%
Diaporthe Seed Decay	3	0	-100.0%
Stem Canker (*Diaporthe spp.*)	3	0	-100.0%
Soybean Cyst Nematode	4	1	-75.0%
Verticillium Wilt	4	1	-75.0%
Charcoal Rot	6	3	-50.0%
Sudden Death Syndrome	2	1	-50.0%

Pathogens Showing Increase

Several pathogens showed concerning increases: brown stem rot (+100.0%), *Stemphylium* leaf blight (+100.0%, 4 to 8 occurrences), *Drechslera* blight (+100.0%), anthracnose stem blight (+50.0%), *Phytophthora* root/stem rot (+33.3%), leaf spot (+33.3%), soft rot (+33.3%), and reniform nematode (+14.3%). Frogeye leaf spot appeared exclusively in treated plots (4 new occurrences). The late-season pathogen increase (+8.8% at V7) suggests declining treatment efficacy as the season progresses, warranting continued monitoring.

15. INTEGRATED ANALYSIS

The integrated cross-domain correlation analysis examined 1,128 pairwise relationships between soil chemistry, functional pathways, microbial community structure, and plant tissue nutrients. Of these, 147 correlations achieved statistical significance ($p < 0.05$), with 71 representing cross-domain relationships that reveal mechanistic linkages between biological processes.

Principal Mechanisms

The integrated analysis suggests that treatment with TNT HEF 2-3-0 appears to operate through community specialization coupled with functional pathway enhancement. The most striking finding is the strong inverse relationship between select functional pathway potential and community diversity metrics. Sulfur oxidation showed exceptionally strong inverse correlation with diversity ($r = -0.984$, $p < 0.0001$), and organic carbon breakdown correlated negatively with diversity ($r = -0.929$, $p = 0.0003$) and evenness ($r = -0.907$, $p = 0.0007$). This pattern suggests that treatment-induced functional changes may occur through community specialization rather than diversification.

Cross-domain correlations between functional pathways and plant tissue nutrients provide evidence for mechanistic linkages between soil microbial function and plant nutritional outcomes. Organic nitrogen breakdown showed positive correlation with tissue nitrogen ($r = +0.829$, $p = 0.006$), supporting a model where treatment stimulates microbial mineralization of organic matter, releasing plant-available nitrogen. Nitrogen fixation correlated positively with tissue magnesium ($r = +0.807$, $p = 0.009$), suggesting coordinated nutrient cycling responses.

Table 15.1: Principal Cross-Domain Correlations

Correlation Pair	r	p-value	Category
Sulfur Oxidation vs Diversity	-0.984	<0.0001	Pathway-Community
Org N Breakdown vs Evenness	-0.941	0.0002	Pathway-Community
Soil Sulfur vs Org C Breakdown	-0.934	0.0002	Soil-Pathway
Org C Breakdown vs Diversity	-0.929	0.0003	Pathway-Community
K Solubilization vs Diversity	-0.885	0.0015	Pathway-Community
Soil Calcium vs Evenness	+0.879	0.0018	Soil-Community
Org N Breakdown vs Tissue N	+0.829	0.0057	Pathway-Tissue
N Fixation vs Tissue Mg	+0.807	0.0086	Pathway-Tissue

Note: Correlations computed using paired treatment response method (n = 9 stage-zone paired observations).

Temporal Dynamics

Treatment effects showed progressive development across growth stages. V2 showed early pathogen suppression (-42.4%) with substantial soil potassium mobilization (+78.1%). V4 demonstrated peak pathway differentiation, with significant nitrification potential enhancement ($p = 0.045$), significant soil calcium increase ($p = 0.008$), and continued pathogen suppression (-46.2%). V7 showed translation to plant outcomes with significant tissue calcium ($p = 0.014$) and significant phosphorus solubilization potential ($p = 0.013$), alongside pathogen equilibration (+8.8%).

Strengths and Constraints

Strengths of treatment with TNT HEF 2-3-0 included: strong early-season pathogen suppression (V2: -42.4%, V4: -46.2%); complete elimination of key soybean pathogens (Diaporthe seed decay, stem canker, brown spot); significant soil to plant calcium transfer (+39.2% soil at V4, +15.6% tissue at V7); significant mid-season nitrification enhancement ($p = 0.045$ at V4); enhanced biocontrol fungi (+129.5% *Trichoderma*, +125.1% fungal biocontrol guild); and increased bacterial nutrient cycling (+32.6%).

Constraints included: nitrogen-fixing bacterial decline (-47.6% guild, -61.4% *Bradyrhizobium*); late-season pathogen equilibration (+8.8% at V7); mycorrhizal

fungi decline (-25.4%); emergence of frogeye leaf spot in treated plots (4 occurrences); and increased Stemphylium leaf blight (+100%).

Management Implications

The *Bradyrhizobium* decline may warrant attention; nodule counts at R1-R2 growth stages would help assess nodulation status. Supplemental inoculant application may be considered to compensate for reduced nitrogen-fixing capacity. The late-season pathogen increase suggests that split application (planting plus V3-V4) could be evaluated to maintain pathogen suppression through reproductive growth.

Limitations

The sample size of n = 3 per treatment per stage limits statistical power for detecting moderate effects, and the single-site design cannot separate treatment effects from site-specific patterns. The inverse diversity-function correlations observed here warrant further investigation across larger sample sizes to determine generalizability. Yield data were not available to correlate nutrient and pathway effects with agronomic outcomes.

16. CONCLUSION

This trial evaluated the effects of in-furrow application of TNT HEF 2-3-0 on soybean rhizosphere microbiome composition, soil nutrient cycling, and plant nutrient uptake at Falor Farm Center during the 2025 growing season. The data suggests that TNT HEF 2-3-0 treatment exhibited a time-dependent response pattern characterized by three distinct phases: early-season pathogen suppression and potassium mobilization (V2), mid-season functional pathway stability and soil calcium enrichment (V4), and late-season translation of soil benefits to plant tissue outcomes (V7).

Variability among samples resulted in limited statistical significance in treatment responses. The most robust findings included significant soil calcium enhancement at V4 (+39.2%, p = 0.008) that successfully translated to significant tissue calcium increase at V7 (+15.6%, p = 0.014), demonstrating a complete soil-to-plant nutrient transfer pathway. Functional metagenomic analysis indicated significant nitrification potential enhancement at V4 (+2 percentile points, p = 0.045) and phosphorus solubilization potential at V7 (+14 percentile points, p = 0.013). Early-season pathogen suppression was substantial, with total pathogen occurrence reduced by 42.4% at V2 and 46.2% at V4, including complete elimination of several key soybean pathogens.

However, the data also revealed potential constraints that warrant consideration. The 47.6% decline in nitrogen-fixing bacterial guild abundance, driven primarily by a 61.4% reduction in *Bradyrhizobium*, represents a concern for biological nitrogen fixation capacity in soybean systems. Additionally, relative abundance of mycorrhizal fungi among the top 20 most abundant fungal genera declined by 25.4%, which may affect phosphorus acquisition through symbiotic pathways. Late-season pathogen equilibration (+8.8% at V7) and emergence of frogeye leaf spot in treated plots suggest that pathogen suppression benefits may diminish over time.

The correlation analysis revealed that functional pathway enhancement appears to occur through community specialization rather than diversification, as indicated by strong inverse relationships between microbial diversity metrics and pathway cycling potential for some nutrients. This pattern suggests that treatment-induced functional changes may involve trade-offs between community diversity and specialized functional capacity.

Study limitations include small sample size (n = 3 per treatment per stage) and single-site design, which constrain statistical power and generalizability. Future research should evaluate split application timing to maintain late-season pathogen suppression, assess nodulation status to determine impacts on biological nitrogen fixation, and include yield measurements to correlate microbiome and nutrient effects with agronomic outcomes.

REFERENCES

Babalola, O. O., Omotayo, O. P., & Igiehon, N. O. (2021). Survey of maize rhizosphere microbiome using shotgun metagenomics. Microbiology Resource Announcements, 10(3), e01309-20.

Berendsen, R. L., Pieterse, C. M. J., & Bakker, P. A. H. M. (2012). The rhizosphere microbiome and plant health. Trends in Plant Science, 17(8), 478-486.

Haney, R. L., Haney, E. B., Smith, D. R., Harmel, R. D., & White, M. J. (2018). The soil health tool - Theory and initial broad-scale application. Applied Soil Ecology, 125, 87-92.

Harman, G. E., Howell, C. R., Viterbo, A., Chet, I., & Lorito, M. (2004). Trichoderma species - Opportunistic, avirulent plant symbionts. Nature Reviews Microbiology, 2(1), 43-56.

Mendes, R., Garbeva, P., & Raaijmakers, J. M. (2013). The rhizosphere microbiome: Significance of plant beneficial, plant pathogenic, and human pathogenic microorganisms. FEMS Microbiology Reviews, 37(5), 634-663.

Richardson, A. E., & Simpson, R. J. (2011). Soil microorganisms mediating phosphorus availability: Update on microbial phosphorus. Plant Physiology, 156(3), 989-996.

Trivedi, P., Leach, J. E., Tringe, S. G., Sa, T., & Singh, B. K. (2020). Plant-microbiome interactions: From community assembly to plant health. Nature Reviews Microbiology, 18(11), 607-621.

Vessey, J. K. (2003). Plant growth promoting rhizobacteria as biofertilizers. Plant and Soil, 255(2), 571-586.